HHS Public Access

Author manuscript

J Bone Miner Res. Author manuscript; available in PMC 2017 September 01.

Published in final edited form as:

J Bone Miner Res. 2016 September ; 31(9): 1688–1700. doi:10.1002/jbmr.2854.

Macrophage migration inhibitory factor (MIF) supports homing of osteoclast precursors to peripheral osteolytic lesions

Alexandru Movila[1], **Takenobu Ishii**[1,2], **Abdullah Albassam**[1,3,4], **Wichaya Wisitrasameewong**[1,3,5], **Mohammed Howait**[1,4], **Tsuguno Yamaguchi**[1,6], **Montserrat Ruiz-Torruella**[1], **Laila Bahammam**[4], **Kazuaki Nishimura**[1,7], **Thomas Van Dyke**[1], and **Toshihisa Kawai**[1,3,*]

[1]The Forsyth Institute, Department of Immunology and Infectious Diseases, Cambridge, MA, USA [2]Tokyo Dental College, Department of Orthodontics, Tokyo, Japan [3]Harvard School of Dental Medicine, Boston, MA, USA [4]King Abdulaziz University, Faculty of Dentistry, Jeddah, Saudi Arabia [5]Chulalongkorn University, Faculty of Dentistry, Department of Periodontology, Bangkok, Thailand [6]Research and Development Headquarters, LION Corporation, 100 Tajima Odawara, Kanagawa, Japan [7]Tohoku University, Graduate School of Dentistry, Sendai, Japan

Abstract

By binding to its chemokine receptor CXCR4 on osteoclast precursor cells (OCPs), it is well known that SDF-1 promotes the chemotactic recruitment of circulating OCPs to the homeostatic bone remodeling site. However, the engagement of circulating OCPs in pathogenic bone resorption remains to be elucidated. The present study investigated a possible chemoattractant role of MIF, another ligand for CXCR4, in the recruitment of circulating OCPs to the bone lytic lesion. To accomplish this, we used Csf1r-eGFP-KI mice to establish an animal model of Polymethyl methacrylate (PMMA) particle-induced calvarial osteolysis. In the circulating Csf1r-eGFP+ cells of healthy Csf1r-eGFP-KI mice, Csf1r+/CD11b+ cells showed a greater degree of RANKL-induced osteoclastogenesis compared to a subset of Csf1r+/RANK+ cells *in vitro*. Therefore, Csf1r-eGFP+/CD11b+ cells were targeted as functionally relevant OCPs in the present study. While expression of the two cognate receptors for MIF, CXCR2 and CXCR4, was elevated on Csf1r+/CD11b+ cells, transmigration of OCPs toward recombinant MIF *in vitro* was facilitated by ligation with CXCR4, but not CXCR2. Meanwhile, the level of PMMA-induced bone resorption in calvaria was markedly greater in wild-type mice compared to that detected in MIF-KO mice. Interestingly, in contrast to the elevated MIF, diminished SDF-1 was detected in a particle-induced bone lytic lesion of wild-type mice in conjunction with an increased number of infiltrating CXCR4+ OCPs. However, such diminished SDF-1 was not found in the PMMA-injected calvaria of MIF-KO mice. Furthermore, stimulation of osteoblasts with MIF *in vitro* suppressed their production of SDF-1, suggesting that MIF can down-modulate SDF-1 production in bone tissue.

*Corresponding author: Toshihisa Kawai, DDS, PhD, Address: Forsyth Institute, Department of Immunology and Infectious Diseases, 245 First Street, Cambridge, MA 02142, USA, Tel: +1-617-892-8317, tkawai@forsyth.org.

Conflicts of Interest

No conflicts of interest are reported.

Authors' roles: AM and TK designed the project; AM, TI, AA, WW, MH, TY, MR-T, LB, KN, and TK performed data collection; AM, TVD and TK performed data interpretation; AM and TK wrote the manuscript.

Systemically administered anti-MIF neutralizing mAb inhibited the homing of CXCR4+ OCPs, as well as bone resorption, in the PMMA-injected calvaria, while increasing locally produced SDF-1. Collectively, these data suggest that locally produced MIF in the inflammatory bone lytic site is engaged in the chemoattraction of circulating CXCR4+ OCPs.

Keywords

MIF; SDF-1; CXCR4; osteoclast precursors; particle-induced osteolytic lesions

Introduction

The response of monocytes to local irritants, such as wear debris particles generated from implant device after total joint arthroplasty, is thought to cause peripheral osteolytic lesion. Growing evidence suggests that the inflammation elicited by wear debris particles promotes migration of osteoclast precursors (OCP) to the osteolytic lesion, while upregulating osteoclastogenesis at the site of inflammation [1–3]. Although these events promote bone resorption, the molecular mechanisms underlying the migration of OCPs remain to be elucidated.

Classical consensus has supported the idea that osteoclasts complete their life cycle in the microenvironment of bone surface. However, accumulated lines of evidence suggest that osteoclast lineage cells, especially OCPs, circulate in the blood stream [4]. It has been demonstrated that monocyte chemoattractant protein-1 (MCP-1), a chemokine which binds to the CCR2 receptor, is associated with the local migration of OCPs to particle-induced lesions [5, 6]. Furthermore, chemotactic recruitment of OCPs to blood circulation is dynamically controlled by sphingosine-1-phosphate (S1P), a chemoattractant factor abundantly available in the blood, which facilitates the migration of OCPs expressing S1PR1 and S1PR2 receptors [7, 8]. Contrary to S1P-mediated migration of OCPs to blood circulation, it is reported that stromal cell-derived factor-1 (SDF-1)/CXCL12, as well as CX3CL1, or fractalkine, both produced in bone marrow, are engaged in the homing of OCPs to bone marrow by ligation with CXCR4 and CX3CR1 receptors, respectively [9, 10].

Accumulated lines of evidence indicate that macrophage migration inhibitory factor (MIF), a pleiotropic proinflammatory protein involved in the development of various bone pathologies, including wear debris-induced osteolysis, elicits chemoattraction for leukocytes via interaction with CD74, CXCR2, and CXCR4 cell receptors [11–18]. Nonetheless, it is still not known if MIF is engaged in the chemotaxis of OCPs to peripheral bone resorption lesions.

Among these three known receptors for MIF, CD74, a single-pass type II membrane protein, also known as MHC class II invariant chain (Ii), does not appear to play a role in MIF-mediated migration of leukocytes by itself, while the complexes of CD74 with the classical trafficking receptors, CXCR2 and CXCR4, are engaged in leukocyte recruitment [14, 19]. Interestingly, the MIF/CD74 axis has been implicated in the promotion of osteoclastogenesis [20, 21]. CXCR2, an IL-8 (CXCL8) receptor, is expressed on the surface of neutrophils, but it is also expressed on the surface of monocytes, a source of OCPs. While

it is unlikely that IL-8/CXCR2 axis elicits a signal required for migration of monocytes [22, 23], MIF/CXCR2 axis is reported to be involved in the arrest and chemotaxis of these cells [14]. However, the possible role of CXCR2 in the recruitment of OCPs to an osteolytic lesion remains unclear. On the other hand, the relevance of chemotactic receptor CXCR4 in the migration of OCPs under physiological conditions has been reported [9]. Moreover, a recent study showed that CXCR4 expression is upregulated on the surface of leukocytes in response to the challenge with metallic wear debris in both *in vitro* and *in vivo* contexts [24]. Nevertheless, to the best of our knowledge, no study has addressed the involvement of the MIF/CXCR4 axis in the induction of OCP chemotaxis.

In the present study, we report that MIF/CXCR4 axis does play a key role in the homing of OCPs to particle-induced osteolysis lesion. Using a mouse model of PMMA-induced osteolysis, anti-MIF neutralizing mAb as well as MIF-KO mice were employed to establish the role of locally produced MIF in homing of CXCR4+ OCPs to bone resorption lesion.

Material and Methods

Mouse strain and anesthesia procedures

The experimental procedures were approved by the Institutional Animal Care and Use Committee (IACUC) at the Forsyth Institute. MIF-knockout (KO) mice, CSF1r-eGFP knock-in (KI) mice and their wild-type (WT) (C57BL/6J) mice were used in this study (6–8 weeks; body weight 25–30 g). CSF1r-eGFP-KI and WT mice were obtained from the Jackson Laboratory (Bar Harbor, ME, USA), and MIF-KO mice were generously donated by Dr. Satoskar (Ohio State University). Animals were kept in a conventional room with a 12-hour light-dark cycle at constant temperature.

Murine particle-induced calvarial osteolysis model

After mice were anaesthetized with ketamine (80 mg/kg) and xylazine (10 mg/kg), Poly(methyl methacrylate) PMMA particles (mean diameter 6.5 μm) (Bangs Laboratories, Fishers, IN) suspended in PBS were injected subcutaneously over the calvarial bone by using a 1 ml Tuberculin syringe attached with a 28G × ½″ needle (Covidien, Inc., Costa Mesa, CA). Control animals received sham injection of PBS (150 μl/site). The site of PMMA suspension in PBS or PBS along injection was adjusted to the midline and one millimeter anterior from the line connecting the ears.

Particle preparation

To prepare an injection suspension of PMMA particles, 10 mg of particles were washed three times in 1 ml of 70% ethanol (molecular biology grade; Sigma-Aldrich) at room temperature. Then the particles were washed in sterile PBS three times and resuspended in 150 μl sterile PBS. The suspension was stored at 4°C not more than one week. All particle preparations were processed under sterile conditions.

μCT analysis

Seven days after placement of PMMA particles, mice were sacrificed, and osteolysis induced in the calvariae was evaluated *ex vivo* by using a SCANCO μCT 40 scanner. A 3-D reconstruction was performed using μCT 40 evaluation software.

Isolation of mononuclear cells

Splenocytes—A mouse spleen was collected and placed into a nylon cell strainer (70 μm; Thermo Fisher Scientific, Waltham, MA). Using the plunger end of the syringe, the spleen was mashed through the cell strainer into a conical tube. Mononuclear cells were isolated using density gradient centrifugation in Histopaque® 1083 (Sigma-Aldrich, St. Louis, MO). Finally, lysis buffer (BioLegend, San Diego, CA) was used to destroy red blood cells.

Calvarial tissue derived mononuclear cells—Murine calvariae were harvested from particle-injected and control animals and placed in PBS on ice. Using a SMZ745T Nikon dissecting microscope (Tokyo, Japan), the dura mater was carefully removed and finely minced into small fragments with sterile scissors (Fine Science Tools) and homogenized using a tissue grinder (Thermo Scientific™). Then, mononuclear cells were isolated from mouse calvariae using a previously published protocol [25] with Histopaque® 1083 gradient centrifugation.

Synovial-like peri-prosthetic membranes derived mononuclear cells—Peri-prosthetic membranes were dissected from the PMMA-induced calvaria lesions and were digested with Collagenase D (Roche, Basel Switzerland). Mononuclear cells were isolated as described above.

Multicolor flow cytometry and FACS sorting

Multicolor flow cytometry of OCPs—Isolated mononuclear cells from murine CSF1r-eGFP-KI calvarial tissues were incubated with anti-mouse CD16/32 (Fc-blocking antibody, Ab) and then stained with anti-CD11b conjugated to Pacific blue, anti-CXCR2 conjugated to Alexa 647, and anti-CXCR4 conjugated to PE Abs (BioLegend, San Diego, CA) to characterize OCPs as $eGFP^+CD11b^+$ cells. Cells were acquired on the BD FACSAria™ II Cell Sorter (BD Biosciences, Franklin Lakes, NJ) and analyzed with FlowJo (ver. 10) software (Tree Star, Ashland, OR).

Multicolor flow cytometry of synovial-like periprosthetic membrane cells—Isolated mononuclear cells were incubated with anti-mouse CD16/32 and then stained with anti-CD45 conjugated to FITC, anti-CD11b conjugated to PE/Cy7, anti-F4/80 conjugated to Alexa 647 Abs (BioLegend) to characterize macrophages as $CD45^+CD11b^+F4/80^+$ cells.

Fluorescence Activated Cell Sorting (FACS)—Mononuclear cells isolated from the spleen of CSF1r-eGFP mice were reacted with anti-CD11b conjugated to Pacific blue and RANK-biotin/avidin-APC/Cy7 Abs in the presence of Fc-blocking Ab (BioLegend). Staining with 7-AAD (BioLegend) was used as a marker for live/dead cells. Cells were then submitted to FACS using the BD FACSAria™ II Cell Sorter.

Chemotaxis assay

Altogether, 5×10^5 FACS-sorted $eGFP^+CD11b^+$ OCPs isolated from the spleen of CSF1r-eGFP-KI mice were loaded in the upper chamber of a transwell culture insert with a pore size of 8 μm (Corning Inc., Corning, NY). Filters were transferred into the wells containing medium (α-MEM, 10% fetal bovine serum, FBS) in the presence or absence of various concentrations of recombinant mouse MIF and SDF-1 proteins (both from BioLegend). To test the effects of chemical inhibitors of CXCR2 or CXCR4 on chemotaxis in response to various concentrations of MIF or SDF-1, SB225002 (100 ng/ml) or plerixafor (100 ng/ml, trade name Mozobil) (both from Cayman Chemical, Ann Arbor, MI), respectively, were used. PBS alone was used as control. The transwell chambers were incubated for 12 hours at 37°C, and the number of cells transmigrating into the lower chamber were counted microscopically, followed by calculation of the chemotactic index as described [26].

RANKL-induced osteoclastogenesis in vitro

Cell populations sorted by FACS or $eGFP^+CD11b^+$ OCPs collected from the lower chamber of a transwell device were seeded in 96-well plates at a density of 1×10^4 cells/well in α-MEM medium (Life Technologies, Carlsbad, CA) containing 10% FBS (Atlanta Biologicals, Norcross, GA) with 30 ng/mL of M-CSF (BioLegend) and 50 ng/ml RANKL (ProSpec, East Brunswick, NJ). OCPs which were stimulated by either MIF or SDF-1 in the course of transmigration were continuously stimulated with the same chemoattractant in the course of RANKL-induced osteoclastogenesis. Five days later, cells were stained for tartrate-resistant acid phosphatase (TRAP) using a leukocyte acid phosphatase kit (Sigma). TRAP-positive (TRAP+) cells with more than three nuclei were considered as osteoclasts. TRAP+ multinuclear cells were counted, and the results were expressed as numbers per well.

Stimulation of bone marrow derived macrophages by PMMA particles in vitro

Mononuclear bone marrow cells isolated from femur and tibia of WT mice were seeded into 24-well plates (5×10^5 cells/well) in α-MEM supplemented with 10% FBS and 30 ng/ml M-CSF (Biolegend). After incubation for 3 days, fresh medium containing 2.5×10^{-3} % (w/v) PMMA particles and 30 ng/ml M-CSF was applied. No particle containing medium served as a control. The cells were stimulated for 24 h and then conditioned medium was collected and evaluated by ELISA.

Effects of plerixafor on OCPs mobilization in vivo

Immediately after PMMA particles placement, groups of CSF1r-eGFP-KI mice were injected subcutaneously (s.c.) with sterile PBS or plerixafor solution in PBS at 5 mg/kg every 24 hours [27]. At day 3, calvaria tissues were collected and evaluated by multicolor flow cytometry as described above.

Design of anti-MIF neutralizing mAb

A monoclonal antibody (mAb) to mouse MIF was developed as described elsewhere [28, 29]. Briefly, 8-week-old BALB/c mice were immunized with highly specific peptide sequence of mouse MIF protein (MIF-peptide: SGTNDPCALCSLHSIGKI) which was designed using BLAST search. A panel of hydridomas resulting from the cell fusion between NS-O

myeloma and splenocytes of immunized mice were subsequently evaluated for specificity to the MIF-peptide as well as recombinant MIF. After cloning of the antibody-producing hybridomas, we obtained one hybridoma which produced MIF-specific mAb (IgG1). The specificity of anti-MIF mAb was confirmed in the ELISA; the binding of anti-MIF mAb to recombinant MIF protein that was coated on ELISA plate was only inhibited by MIF-peptide and recombinant MIF, but not by control irrelevant peptide sequences.

Total proteins isolation from murine calvariae, and long bone tissues, and ELISA

Mouse calvariae and femur bones were collected from euthanized WT and MIF-KO animals and weighed. Then bones were mechanically homogenized on ice with a mortar and pestle in PBS with 0.05% Tween 20 in the presence of 10 μg/ml of ethylenediaminetetraacetic acid (EDTA)-free protease inhibitor cocktail (Thermo Scientific™). The suspension was centrifuged at 1500 rpm. Concentrations of MIF, SDF-1, and TNF-α proteins were measured from the collected supernatant using commercial sandwich ELISA kits from R&D (Minneapolis, MN) and Biolegend, respectively, according to the manufacturer's recommendation.

Effects of MIF stimulation on SDF-1 production by murine MC3T3 cells

Mouse MC3T3 cells were (24-well plates; 1×10^5 cells/well) stimulated *in vitro* by various concentrations of mouse MIF recombinant protein in the presence or absence of anti-MIF mAb or IgG control (both 100 μg/ml). In some experiments plerixafor (100 ng/ml) was used to block CXCR4 receptor. The concentration of SDF-1 was measured by ELISA as described above.

Histological analyses and immunohistochemistry

Tissue decalcification—Calvariae were dissected and fixed in 4% formaldehyde overnight and then decalcified in 10% EDTA (Thermo Fisher Scientific) for 2 weeks at 4°C. Decalcified samples were dehydrated in graded alcohols and embedded in paraffin. Frontal calvarial sections 6-μm in thickness centered on the sagittal suture were obtained for histological analysis.

TRAP staining—To stain TRAP+ OCs, sections were first incubated in 0.2M acetate buffer containing 50 mM L-(+)-Tartaric acid (Sigma) at room temperature and then in TRAP staining solution (0.2 M acetate buffer, 50 mM L-(+)-Tartaric acid, 0.5 mg/ml Naphthol AS-MX phosphate, 1.1 mg/ml Fast Red ASTR salt; Sigma) at 37°C. Finally, the sections were counterstained with hematoxylin solution (Sigma) at room temperature.

MIF immunohistochemistry—Calvarial sections were first incubated in a rabbit anti-MIF polyclonal Ab (clone N1C3) at 1:500 (GeneTex, Irvine, CA), then in a horseradish-peroxidase conjugated avidin-biotin complex in Vectastain Elite ABC Kit, and staining was resolved with DAB peroxidase substrate kit (Vector Laboratories) according to the to the manufacturer's recommendation. Finally sections were counterstained with 0.1% Fast green (Sigma) in PBS. To evaluate the anti-MIF antibody binding specificity, anti-MIF mAb was reacted with the section of kidney isolated from WT as well as MIF-KO, based on the report

that demonstrated strong positive staining pattern of MIF in the epithelial cells of the kidney proximal tubules [30] (Suppl. Fig. 1).

Statistical analysis

Data are displayed as mean ± SEM. Statistical significance was evaluated using a one-way ANOVA with post hoc Tukey's test. A $p < 0.05$ was considered statistically significant. Data were analyzed using PAST 2.1 statistical software.

RESULTS

Immunophenotypic characterization of OCPs isolated from Csf1r-eGFP-KI mice

Using Csf1r-eGFP-KI mice whose monocyte-lineage cells predominantly express eGFP, Ishii et al., demonstrated that OCPs migrate in response to S1P [8]. As such, this transgenic strain could be used as an animal model to elucidate the molecular mechanisms underlying the migration of OCPs to peripheral osteolytic lesions. However, since Csf1r (also called CD115) is a phenotypic marker for monocyte-lineage cells, $eGFP^+$ cells can either be OCPs or non-OCPs. Moreover, no consensus has been reached on immunophenotypic markers characteristic of murine OCPs. Therefore, on the basis of these results, as well as other published reports [31–33], Csf1r-eGFP, RANK, and CD11b were selected in the present paper as potential markers for OCPs in Csf1r-eGFP-KI mice.

First, among $Csf1r\text{-}eGFP^+$ mononuclear cells, the expression patterns of RANK and CD11b were evaluated using flow cytometry. Four distinct subpopulations were identified by FACS, including $RANK^-/CD11b^-$, $RANK^+/CD11b^-$, $RANK^-/CD11b^+$ and $RANK^+/CD11b^+$, and separated using cell sorting system. Each subset was *ex vivo*-stimulated with RANKL and M-CSF (Fig. 1A). After 5 days of RANKL stimulation, the highest number of TRAP+ multinuclear cells was detected in the $eGFP^+CD11b^+RANK^-$ subset, followed by the $eGFP^+CD11b^+RANK^+$ population, while the other two subsets showed few, or no, TRAP+ multinuclear cells (Fig. 1B and C). These results indicate that $CSF1r\text{-}eGFP^+CD11b^+$ cells, both $RANK^-$ and $RANK^+$, isolated from the spleen of Csf1r-eGFP-KI mice could be characterized as OCPs.

According to these data, RANK was not included as a marker for immunophenotyping OCPs in Csf1r-eGFP-KI mice, and only eGFP and CD11b were used. Thus, subpopulations of $eGFP^-/CD11b^-$, $eGFP^+/CD11b^-$, $eGFP^+/CD11b^+$ and $eGFP^-/CD11b^+$ were FACS-sorted and then RANKL/M-CSF-stimulated as described above (Fig. 1D). As expected, only $eGFP^+CD11b^+$ cells became TRAP+ OCs (Fig. 1E & F).

Finally, the expression of MIF receptors, CXCR2 and CXCR4, on the surface of $eGFP^+CD11b^+$ OCPs, as well as other FACS-sorted subpopulations, was evaluated. Our results show that 20.5% and 23.5% of OCPs were positive for CXCR2 and CXCR4, respectively (Fig. 1G & H).

Collectively, these data indicate that 1) $CSF1r\text{-}eGFP^+CD11b^+$ cells can be characterized as OCPs in Csf1r-eGFP-KI mice and 2) they express both CXCR2 and CXCR4 receptors on their surface in equal amounts.

Ligation of CXCR4 receptor with MIF promotes chemotaxis of OCPs and subsequent osteoclastogenesis in vitro

Since CXCR4 is a receptor for both MIF and SDF-1, we tested the effects of both chemokines on freshly FACS-sorted $eGFP^+CD11b^+$ OCPs using a transwell migration device *in vitro*. As expected, both chemokines showed a dose-dependent chemotactic effect on OCPs (Fig. 2A). However, higher concentrations of MIF significantly enhanced ($p = 0.016$) the transmigration activity of OCPs compared to stimulation with SDF-1 (Fig. 2A).

We then compared the ability of transmigrated OCPs to become OCs in response to MIF, as well as SDF-1 stimulations, in RANKL-induced osteoclastogenesis. The number of TRAP+ osteoclasts formed from the transmigrated OCPs in response to MIF stimulation was significantly higher ($p = 0.037$) when compared to stimulation with SDF-1 (Fig. 2B).

Next, the effects of a newly developed anti-MIF-mAb, as a prospective drug, on MIF- and SDF-1-elicited chemotaxis of OCPs were tested *in vitro*. It is important to note that neither anti-MIF-mAb nor control isotype-matched control mAb affected RANKL-induced osteoclastogenesis *in vitro* (Fig. 2C).

The number of transmigrated OCPs in response to MIF was significantly ($p = 0.002$) suppressed by the anti-MIF neutralizing mAb (Fig 2D). Further, the anti-MIF-mAb also significantly reduced ($p = 0.002$) the amount of TRAP+ OCs formed from the transmigrated OCPs (Fig. 2E). In contrast, we observed no significant effects on OCP chemotaxis ($p = 0.36$) or RANKL-induced osteoclastogenesis ($p = 0.37$) by the simultaneous presence of SDF-1 recombinant protein and anti-MIF-mAb (Fig. 2D & E).

Finally, to evaluate the possible engagements of CXCR2 and CXCR4 receptors in MIF- and SDF-1-elicited OCP migration, chemotaxis assays were carried out in the presence or absence of SB225002 or plerixafor, chemical antagonist for CXCR2 or CXCR4, respectively. Chemotaxis of OCPs in response to MIF and SDF-1 was unaffected by the CXCR2 antagonist, SB225002 (Fig. 3A & B). In contrast, plerixafor significantly suppressed the transmigration of OCPs in response to MIF ($p = 0.0018$) and SDF-1 ($p < 0.001$) *in vitro* (Fig. 3A & B). Further, plerixafor also dramatically reduced the number of OCs from both MIF- and SDF-1-stimulated cells (Fig. 3C). In addition, SB225002 slightly reduced the amount of TRAP+ osteoclasts in the MIF-, but not SDF-1-, stimulated wells (Fig. 3C).

These observations indicated that ligation of MIF and SDF-1 with CXCR4 receptor promotes transmigration of OCPs, as well as osteoclastogenesis, *in vitro*. However, compared to SDF-1, MIF elicited signals that promoted more active transmigration and fusion of OCPs. Further, anti-MIF-mAb effectively neutralized the biological functions of MIF only, but not SDF-1 *in vitro*.

MIF plays a role in the development of peripheral bone lesions in vivo

To address whether MIF plays a role in the development of peripheral bone lesions *in vivo*, we first induced osteolysis lesion in the calvaria of WT and MIF-KO mice via local injection of PMMA particles (PBS suspension) or control PBS. The changes of bone surface structure

were monitored using μCT. At seven days after the injection of control PBS, no sign of osteolysis were detected in WT mice (Suppl. Fig. 2 A). The injection of PMMA induced a severe bone resorption in the calvaria of WT mice (Suppl. Fig. 2 B). In contrast, lesser level of osteolysis was observed in the MIF-KO mice that received PMMA injection (Suppl. Fig. 2 C). These results indicated that MIF plays an important role in development of the particle-induced osteolysis lesion.

Next, we measured concentrations of MIF and SDF-1 proteins in calvarial tissues of control and particle-induced lesions using ELISA. In calvarial tissues of WT mice, the level of MIF was significantly elevated in the group that received PMMA injection ($p = 0.0013$), whereas the level of MIF in remote site of femur bone was not affected ($p = 0.62$) by PMMA injection to calvaria (Fig. 4A & B). In contrast, the amount of SDF-1 was significantly downregulated ($p < 0.001$) in PMMA-induced calvaria tissues compared to the control in WT animals (Fig. 4C). Further, similar expression patterns of SDF-1 (p=0.62) was observed in non-treated femurs of control WT mice as well as those received PMMA injection in the calvaria (Fig. 4D). On the other hand, in terms of MIF-KO mice, no significant fluctuations of SDF-1 concentrations between osteolytic calvarial lesions and healthy calvariae were observed (Fig. 4C). Similarly, comparable amounts of SDF1 were detected between the femur of control non-treated and that of mice received calvarial injection with PMMA (Fig. 4D). Altogether, these results indicated that PMMA injection into calvaria can induce local production of MIF while suppressing the expression of SDF1, whereas such a local PMMA injection does not affect the MIF and SDF1 productions in the peripheral bones.

Next, effects of systemic administration with anti-MIF-mAb on the development of osteolytic lesions were examined. According to the μCT evaluation, no sign of osteolysis was detected in control mice that received an injection of PBS (Fig. 5A). In contrast, the size of osteolytic lesion in the mouse group that received PMMA particles and control IgG was larger than that found in the group of mice received PMMA particles and anti-MIF neutralizing mAb (Fig. 5B & C). Furthermore, the number of TRAP+ cells and inflammatory infiltrates at the lesion was found elevated in the mice received PMMA particle and control IgG (Fig. 5E & G) compared to the groups that received control PBS injection alone (Fig. 5D & G) or PMMA particles and anti-MIF-mAb (Fig. 5F & G).

Since anti-MIF-mAb suppressed the development of osteolytic lesion along with increased TRAP+ cells and inflammatory infiltrates (Fig. 5), we evaluated effects of anti-MIF-mAb on the production of MIF and SDF-1 in the calvaria injection site. As expected, the amount of MIF was significantly elevated ($p < 0.001$), while SDF-1 was reduced in the bone lytic lesion that received PMMA and control IgG injection compared to the group that received control PBS alone (Fig. 6A & B). Importantly, the administration of anti-MIF-mAb significantly reduced the concentration of MIF in the PMMA-induced calvaria lesion (Fig. 6A). Very interestingly, the amount of SDF-1 in calvarial lesions of anti-MIF-mAb treated group was significantly higher than that detected in the group that received PMMA and control IgG (Fig. 6B). The concentration of MIF in femur was decreased in the group that received anti-MIF-mAb (Fig. 6C), suggesting the effectiveness of anti-MIF-mAb to neutralize MIF systemically. Contrast to levels of MIF femur, administration with anti-MIF-

mAb did not show any significant differences in the concentration of SDF-1 produced in femur compared to the other two control treatments (Fig 6D).

It is important to note that the PMMA-injected mice those were treated with anti-MIF-mAb showed significantly reduced ($p = 0.026$) amount of pro-inflammatory cytokine TNF-α in osteolytic lesions compared to PMMA-injected mice those received control IgG injection (Suppl. Fig. 3 A). No TNF-α was observed in control femur bones (Suppl. Fig. 3 B).

Then, in order to examine whether neutralization of MIF could affect the recruitment of $CXCR4^+$ OCPs to the particle-induced osteolytic lesion, calvaria tissues of control and PMMA particle-injected mice were systemically treated with control IgG or anti-MIF-mAb and cells infiltrating in the osteolytic lesion were analyzed by multicolor flow cytometry. The injection of PMMA particle increased the infiltration of $eGFP^+CD11b^+$ OCPs (Fig. 7A & B). Systemic administration with anti-MIF-mAb significantly suppressed the infiltration of $eGFP^+CD11b^+$ OCPs in the lesion compared to the group of mice that received control-IgG injection (Fig 7B & C). Furthermore, the elevated incidence of $CXCR4^+$ OCPs in PMMA particle-induced lesions were significantly reduced ($p < 0.001$) by the administration with anti-MIF-mAb treatment (Fig. 7D), suggesting that migration of $CXCR4^+$ OCPs to osteolytic lesion is up-regulated by MIF. In support of this evidence, we also identified that the incidence of $eGFP^+CD11b^+$ OCPs in peripheral calvaria lesions was reduced in response to plerixafor treatment than that detected in control animals (Suppl. Fig. 4). It is important to note that no effect of plerixafor on MIF production in the PMMA particle-induced lesion was detected (Suppl. Fig. 5).

Macrophages of the synovial-like periprosthetic membrane are the main local source of MIF in particle-induced lesions

Since a large number of studies show that a periprosthetic membrane plays a crucial role in production of inflammatory mediators in the context of particle-induced osteolysis [34, 35], we have examined whether MIF is also produced from periprosthetic membrane in response to the stimulation with PMMA-particles. As expected, the periprosthetic membrane of PMMA particle-induced osteolytic lesion showed strong MIF immunohistochemical signal (Fig 8A & B; Suppl. Fig. 1).

Next, we analyzed mononuclear cells isolated from periprosthetic membrane of PMMA-induced osteolytic lesion by multicolor flow cytometry. Among mononuclear cells in the periprosthetic membrane of osteolytic lesion, majority of cells (66.7%) expressed $CD45^+$ hematopoietic origin marker in which 57% of the cells were $CD11b^+F4/80^+$ macrophages (Fig. 8C), suggesting that the majority of cellular infiltrates in the periprosthetic membrane are composed of macrophages. It is noteworthy that significantly ($p < 0.001$) elevated MIF secretion was detected from PMMA stimulated bone marrow derived macrophages *in vitro* (Fig. 8D).

These results indicated that the increased amount of MIF in the PMMA-induced osteolysis lesions are derived from activated macrophages present in periprosthetic membrane.

MIF produced by the periprosthetic membrane cells down-modulate SDF-1 production from osteoblasts in vitro

Because the concentrations of MIF were inversely proportional to SDF-1 produced in osteolytic lesions (Fig 4), we have tested the effects of MIF on the secretion of SDF-1 from osteoblasts, which is the major cellular source of SDF-1 in bone tissue [36]. As expected, addition of the conditioned medium from *ex vivo* cultured periprosthetic membrane cells significantly down-modulated ($p < 0.001$) the SDF-1 release from murine MC3T3 osteoblasts-like cells which was partially abrogated by addition of anti-MIF-mAb ($p = 0.008$) (Fig. 9A). Incubation of MC3T3 cells with various concentrations of mouse recombinant MIF protein significantly ($p < 0.001$) suppressed the production of SDF-1, while such SDF1-suppression effect by MIF was partially restored by the addition of anti-MIF-mAb (Fig. 9B). Finally, to test whether MIF-mediated suppression of SDF-1 production from osteoblasts depends on CXCR4, plerixafor was applied to the MIF-stimulated MC3T3 cells. The results showed that plerixafor can partially inhibit MIF-mediated suppression of SDF production by MC3T3 cells ($p = 0.002$), whereas constitutively produced SDF-1 from osteoblast-like cells was not affected by the addition of plerixafor alone in the absence of MIF (Fig. 9C).

Collectively, these data indicated that MIF can suppress SDF-1 production from osteoblast cells via ligation to its cognate receptor CXCR4, supporting our key finding that MIF/CXCR4 axis plays a major role in the development of particle-induced peripheral osteolytic lesions.

DISCUSSION

In the present study, we showed that OCPs isolated from CSF1r-eGFP mice, characterized as $eGFP^+CD11b^+$ cells, express both MIF's CXCR2 and CXCR4 chemotactic receptors at equivalent levels. Our studies also showed that ligation of both MIF and SDF-1 chemokines to CXCR4, but not CXCR2, receptor triggers chemotaxis of OCPs and enhances osteoclastogenesis. It was further demonstrated that the MIF/CXCR2 axis supports osteoclastogenesis *in vitro*. Although MIF has been a subject of study for several decades, its role in the homing of OCPs to particle-induced bone lesions remains controversial. Thus, it was reported that the ligation of MIF with its CD74 receptor promotes osteoclastogenesis [20, 21]. On the other hand, it was shown that MIF suppresses osteoclastogenesis as well as CD74-KO mice have an increased capacity to form osteoclasts *in vitro* as well as *in vivo* [37, 38]. In the current study it was demonstrated that MIF enhances RANKL-induced osteoclastogenesis *in vitro* as well as plays an important role in recruitment of OCPs to a particle-induced peripheral bone lesion (Fig. 2–8). It has also been clearly demonstrated that MIF binding to its cognate receptors, CXCR2 and CXCR4, promotes leukocyte recruitment to the site of inflammation [14, 39–42]. The ligation of CXCR2 and CXCR4 with IL-8 and SDF-1 ligands, respectively, also promotes leukocyte chemotaxis [43]. However, in terms of chemotaxis of OCPs, thus far, only SDF-1 was reported to plays a chemotactic role for OCPs for their migration to a bone tissue [22, 44–46]. The engagement of CXCR4 for chemotaxis of OCPs in the development of various peripheral osteolytic lesions has only recently been reported [24, 47]. Nonetheless, the

importance of MIF in the migration of $CXCR4^+$ OCPs was never addressed in those studies. Collectively, therefore, our results are supported by lines of evidence showing that CXCR4 signaling regulates chemotaxis of OCPs.

While an earlier clinical study reported elevated MIF expression in the bone that surrounds loosening prosthetic implants [34, 48]. Our results also showed that elevated MIF in the osteolytic lesion is derived from peri-prosthetic membrane which is predominantly infiltrated with activated macrophages (Fig. 8). These results corresponded with earlier reports showing that inflammatory stimuli enhances MIF release from macrophages [49, 50]. In terms of the other ligand for CXCR4, SDF-1, it was reported that expression of SDF-1 is reduced in the local arthritic lesion in a mouse model of TNF-induced arthritis [51], supporting our finding of diminished SDF-1 in the osteolytic lesion (Fig. 4). Very interestingly, inversely proportional relationship between MIF and SDF-1 were detected in a mouse model of particle-induced osteolytic calvarial lesion (Fig. 4). MIF-KO mice demonstrated a reduced size of osteolysis lesion compared to WT mice (Suppl. Fig. 2), while showing the significantly higher level of SDF-1 in PMMA-induced osteolysis lesion than that detected in WT mice (Fig. 4C). In sum, these results suggested that elevated expression of MIF in response to inflammatory (PMMA) stimuli would suppress the SDF-1 in the calvaria tissue.

It was demonstrated that elevated MIF can suppress the production of SDF-1 from osteoblasts partially in a CXCR4-dependent manner *in vitro* (Fig. 9). More specifically, the application of plerixafor, a CXCR4 antagonist, to MIF-stimulated MC3T3 did not sufficiently restore the SDF-1 produced. Such result indicated that other MIF-receptors may be involved in the suppression of SDF-1 production from osteoblasts or that other unknown factor(s) intervene the SDF-1 suppression induced by MIF. Among a various regulatory cytokines, it was reported that transforming growth factor beta (TGF-β) can decrease SDF-1 production from bone marrow stromal cells as well as MC3T3 cells [36, 52]. On the other hand, it was demonstrated that MIF induces TGF-β synthesis in several animal pathophysiological models [53, 54]. In the light of these reports, it is conceivable that TGF-β may be engaged in the MIF-mediated suppression of SDF-1 production in a mouse PMMA-induced osteolysis model. For that reason, additional future investigations are warranted to elucidate the molecular mechanism supporting the MIF-mediated SDF-1 suppression in the context to PMMA-induced inflammatory osteolysis.

Our results partially supported the previous finding by Wright et al., that SDF-1 is involved in the chemoattraction of OCPs to a healthy homeostatic bone remodeling site, but not to pathogenic inflammatory bone resorption site [45]. However, another study reported that SDF-1 is engaged in the recruitment of hematopoietic OCPs to the bone metastasis lesion of giant cell tumor [44]. The latter finding of SDF-1-mediated recruitment of OCPs to inflammatory lesion looks contradictory to the former theory. However, since SDF-1 can form a complex with high mobility group box 1 (HMGB1), an alarmin belonging to the most robust endogenous damage associated molecular patterns (DAMPs), which is widely expressed in tumors and a variety of sterile inflammatory lesions [55–57], it is speculated that SDF-1/HMGB1 complex that should functions differently from SDF-1 by itself may facilitates recruitment of hematopoietic OCPs to the giant cell tumor lesion. While it is true

that the positive effects of HMGB1 on bone resorption are well established [58], the roles played by the HMGB1/MIF complex in the migration of OCPs and osteoclastogenesis are unknown. Because the property of HMGB1 to from complex with both SDF1 and MIF is outside of the scope of the present study, this issue will be addressed in the future studies.

Because our results indicate that MIF plays an important role in the chemotaxis of OCPs and subsequent osteoclastogenesis, as well as the development of particle-induced peripheral osteolytic lesions, we evaluated the effects of MIF inhibition on OCP chemotaxis and the lesion development (Fig. 2–7). Along the line of approach inhibiting MIF's activity, chemical compounds those inhibit the tautomerase activity of MIF were proposed as a strategy to abrogate the proinflammatory actions of MIF [59]. On the other hand, although the genetically engineered knock-in of an allele encoding a tautomerase-deficient MIF did not eliminate the growth-promoting action of the protein [60], fully humanized anti-MIF-mAbs successfully inhibiting the growth of human prostate cancer cells were recently generated [60]. In addition, therapeutic mAbs have captured almost 50% of the best-selling 20 drugs in the U.S. [61]. Notwithstanding these statistics, no studies have reported the effects of anti-MIF-mAb on bone lesions. Therefore, we developed an anti-MIF-mAb and tested its effects on the recruitment of OCPs to peripheral osteolytic lesions. We found that MIF neutralization as well as inhibition of CXCR4 receptor using anti-MIF-mAb and plerixafor, respectively, significantly reduces the number of OCPs at the osteolytic lesion (Fig. 7; Suppl. Fig. 4), supporting an evidence that MIF/CXCR4 axis is involved in recruitment of OCPs to particle-induced bone osteolysis. Results also showed that the bone resorption area of mouse calvariae is reduced in anti-MIF-mAb-treated mice compared to untreated mice (Fig. 5). Moreover, in response to anti-MIF-mAb treatment, the concentration of SDF-1 was increased at the particle-induced bone inflammation area, approaching an amount equal to that found in healthy bones (Fig. 6). SDF-1-elicited chemotaxis of OCPs was unaffected by anti-MIF-mAb treatment (Fig. 2). Therefore, these results suggest that MIF promotes the homing of $CXCR4^+$ OCPs to the bone lesions area, while SDF-1 is engaged in the recruitment of OCPs to healthy bone via ligation with $CXCR4^+$ OCPs. Thus, this newly developed anti-MIF-mAb may represent a potential therapeutic tool for the prevention of peripheral osteolytic lesions.

In conclusion, the present study detected local production of MIF in response to inflammatory stimuli. Results also showed that such chemokine production induces the migration of OCPs to the inflamed osteolytic lesion. In contrast, homeostasis in healthy bone is sustained by the chemoattraction of OCPs by SDF-1 whose expression is, in fact, reduced at the inflamed osteolytic lesion. Taken together, it appears that MIF, but not SDF-1, is engaged in the recruitment of $CXCR4^+$ OCPs in the process of pathological bone resorption.

Supplementary Material

Refer to Web version on PubMed Central for supplementary material.

Acknowledgments

This work was supported by NIH grants T32 DE 7327-12, DE-019917 and DE-018499 from the National Institute of Dental and Craniofacial Research.

References

1. Haynes DR, Crotti TN, Zreiqat H. Regulation of osteoclast activity in peri-implant tissues. Biomaterials. 2004; 25(20):4877–85. [PubMed: 15109848]
2. Gallo J, Goodman SB, Konttinen YT, Raska M. Particle disease: biologic mechanisms of periprosthetic osteolysis in total hip arthroplasty. Innate Immun. 2013; 19(2):213–24. [PubMed: 22751380]
3. Goodman SB. Wear particles, periprosthetic osteolysis and the immune system. Biomaterials. 2007; 28(34):5044–8. [PubMed: 17645943]
4. Kotani M, Kikuta J, Klauschen F, Chino T, Kobayashi Y, Yasuda H, et al. Systemic circulation and bone recruitment of osteoclast precursors tracked by using fluorescent imaging techniques. Journal of immunology. 2013; 190(2):605–12.
5. Gibon E, Ma T, Ren PG, Fritton K, Biswal S, Yao Z, et al. Selective inhibition of the MCP-1-CCR2 ligand-receptor axis decreases systemic trafficking of macrophages in the presence of UHMWPE particles. Journal of orthopaedic research : official publication of the Orthopaedic Research Society. 2012; 30(4):547–53. [PubMed: 21913218]
6. Huang Z, Ma T, Ren PG, Smith RL, Goodman SB. Effects of orthopedic polymer particles on chemotaxis of macrophages and mesenchymal stem cells. Journal of biomedical materials research Part A. 2010; 94(4):1264–9. [PubMed: 20694994]
7. Ishii M, Egen JG, Klauschen F, Meier-Schellersheim M, Saeki Y, Vacher J, et al. Sphingosine-1-phosphate mobilizes osteoclast precursors and regulates bone homeostasis. Nature. 2009; 458(7237):524–8. [PubMed: 19204730]
8. Ishii M, Kikuta J, Shimazu Y, Meier-Schellersheim M, Germain RN. Chemorepulsion by blood S1P regulates osteoclast precursor mobilization and bone remodeling in vivo. The Journal of experimental medicine. 2010; 207(13):2793–8. [PubMed: 21135136]
9. Yu X, Huang Y, Collin-Osdoby P, Osdoby P. Stromal cell-derived factor-1 (SDF-1) recruits osteoclast precursors by inducing chemotaxis, matrix metalloproteinase-9 (MMP-9) activity, and collagen transmigration. Journal of bone and mineral research : the official journal of the American Society for Bone and Mineral Research. 2003; 18(8):1404–18.
10. Koizumi K, Saitoh Y, Minami T, Takeno N, Tsuneyama K, Miyahara T, et al. Role of CX3CL1/fractalkine in osteoclast differentiation and bone resorption. Journal of immunology. 2009; 183(12):7825–31.
11. Gregory JL, Leech MT, David JR, Yang YH, Dacumos A, Hickey MJ. Reduced leukocyte-endothelial cell interactions in the inflamed microcirculation of macrophage migration inhibitory factor-deficient mice. Arthritis and rheumatism. 2004; 50(9):3023–34. [PubMed: 15457472]
12. Cheng Q, McKeown SJ, Santos L, Santiago FS, Khachigian LM, Morand EF, et al. Macrophage migration inhibitory factor increases leukocyte-endothelial interactions in human endothelial cells via promotion of expression of adhesion molecules. Journal of immunology. 2010; 185(2):1238–47.
13. Amin MA, Haas CS, Zhu K, Mansfield PJ, Kim MJ, Lackowski NP, et al. Migration inhibitory factor up-regulates vascular cell adhesion molecule-1 and intercellular adhesion molecule-1 via Src, PI3 kinase, and NFkappaB. Blood. 2006; 107(6):2252–61. [PubMed: 16317091]
14. Bernhagen J, Krohn R, Lue H, Gregory JL, Zernecke A, Koenen RR, et al. MIF is a noncognate ligand of CXC chemokine receptors in inflammatory and atherogenic cell recruitment. Nature medicine. 2007; 13(5):587–96.
15. Singh A, Leng L, Fan J, Gajda M, Brauer R, Fingerle-Rowson G, et al. Macrophage-derived, macrophage migration inhibitory factor (MIF) is necessary to induce disease in the K/BxN serum-induced model of arthritis. Rheumatology international. 2013; 33(9):2301–8. [PubMed: 23503937]
16. Chen Z, Ma T, Huang C, Zhang L, Hu T, Li J. MIF, a potential therapeutic target for rheumatoid arthritis? Rheumatology international. 2014; 34(10):1481–2. [PubMed: 24463567]
17. Madeira MF, Queiroz-Junior CM, Costa GM, Santos PC, Silveira EM, Garlet GP, et al. MIF induces osteoclast differentiation and contributes to progression of periodontal disease in mice. Microbes and infection/Institut Pasteur. 2012; 14(2):198–206. [PubMed: 22016007]

18. Ichiyama H, Onodera S, Nishihira J, Ishibashi T, Nakayama T, Minami A, et al. Inhibition of joint inflammation and destruction induced by anti-type II collagen antibody/lipopolysaccharide (LPS)-induced arthritis in mice due to deletion of macrophage migration inhibitory factor (MIF). Cytokine. 2004; 26(5):187–94. [PubMed: 15157895]
19. Schwartz V, Lue H, Kraemer S, Korbiel J, Krohn R, Ohl K, et al. A functional heteromeric MIF receptor formed by CD74 and CXCR4. FEBS letters. 2009; 583(17):2749–57. [PubMed: 19665027]
20. Fan H, Hall P, Santos LL, Gregory JL, Fingerle-Rowson G, Bucala R, et al. Macrophage migration inhibitory factor and CD74 regulate macrophage chemotactic responses via MAPK and Rho GTPase. Journal of immunology. 2011; 186(8):4915–24.
21. Gu R, Santos LL, Ngo D, Fan H, Singh PP, Fingerle-Rowson G, et al. Macrophage migration inhibitory factor is essential for osteoclastogenic mechanisms in vitro and in vivo mouse model of arthritis. Cytokine. 2015; 72(2):135–45. [PubMed: 25647268]
22. Morohashi H, Miyawaki T, Nomura H, Kuno K, Murakami S, Matsushima K, et al. Expression of both types of human interleukin-8 receptors on mature neutrophils, monocytes, and natural killer cells. Journal of leukocyte biology. 1995; 57(1):180–7. [PubMed: 7829970]
23. Walz A, Meloni F, Clark-Lewis I, von Tscharner V, Baggiolini M. [Ca2+]i changes and respiratory burst in human neutrophils and monocytes induced by NAP-1/interleukin-8, NAP-2, and gro/MGSA. Journal of leukocyte biology. 1991; 50(3):279–86. [PubMed: 1856598]
24. Drynda A, Singh G, Buchhorn GH, Awiszus F, Ruetschi M, Feuerstein B, et al. Metallic wear debris may regulate CXCR4 expression in vitro and in vivo. Journal of biomedical materials research Part A. 2014
25. Bakker AD, Klein-Nulend J. Osteoblast isolation from murine calvaria and long bones. Methods in molecular biology. 2012; 816:19–29. [PubMed: 22130919]
26. Klasen C, Ohl K, Sternkopf M, Shachar I, Schmitz C, Heussen N, et al. MIF promotes B cell chemotaxis through the receptors CXCR4 and CD74 and ZAP-70 signaling. Journal of immunology. 2014; 192(11):5273–84.
27. Broxmeyer HE, Orschell CM, Clapp DW, Hangoc G, Cooper S, Plett PA, et al. Rapid mobilization of murine and human hematopoietic stem and progenitor cells with AMD3100, a CXCR4 antagonist. The Journal of experimental medicine. 2005; 201(8):1307–18. [PubMed: 15837815]
28. Kawai T, Ito HO, Sakato N, Okada H. A novel approach for detecting an immunodominant antigen of Porphyromonas gingivalis in diagnosis of adult periodontitis. Clinical and diagnostic laboratory immunology. 1998; 5(1):11–7. [PubMed: 9455872]
29. Komatsuzawa H, Kawai T, Wilson ME, Taubman MA, Sugai M, Suginaka H. Cloning of the gene encoding the Actinobacillus actinomycetemcomitans serotype b OmpA-like outer membrane protein. Infection and immunity. 1999; 67(2):942–5. [PubMed: 9916112]
30. Bacher M, Meinhardt A, Lan HY, Mu W, Metz CN, Chesney JA, et al. Migration inhibitory factor expression in experimentally induced endotoxemia. The American journal of pathology. 1997; 150(1):235–46. [PubMed: 9006339]
31. Li P, Schwarz EM, O'Keefe RJ, Ma L, Looney RJ, Ritchlin CT, et al. Systemic tumor necrosis factor alpha mediates an increase in peripheral CD11bhigh osteoclast precursors in tumor necrosis factor alpha-transgenic mice. Arthritis and rheumatism. 2004; 50(1):265–76. [PubMed: 14730625]
32. Hayashi H, Nakahama K, Sato T, Tuchiya T, Asakawa Y, Maemura T, et al. The role of Mac-1 (CD11b/CD18) in osteoclast differentiation induced by receptor activator of nuclear factor-kappaB ligand. FEBS letters. 2008; 582(21–22):3243–8. [PubMed: 18775427]
33. Muto A, Mizoguchi T, Udagawa N, Ito S, Kawahara I, Abiko Y, et al. Lineage-committed osteoclast precursors circulate in blood and settle down into bone. Journal of bone and mineral research : the official journal of the American Society for Bone and Mineral Research. 2011; 26(12):2978–90.
34. Purdue PE, Koulouvaris P, Nestor BJ, Sculco TP. The central role of wear debris in periprosthetic osteolysis. HSS journal : the musculoskeletal journal of Hospital for Special Surgery. 2006; 2(2): 102–13. [PubMed: 18751821]
35. Goldring SR, Jasty M, Roelke MS, Rourke CM, Bringhurst FR, Harris WH. Formation of a synovial-like membrane at the bone-cement interface. Its role in bone resorption and implant

loosening after total hip replacement. Arthritis and rheumatism. 1986; 29(7):836–42. [PubMed: 3091038]

36. Jung Y, Wang J, Schneider A, Sun YX, Koh-Paige AJ, Osman NI, et al. Regulation of SDF-1 (CXCL12) production by osteoblasts; a possible mechanism for stem cell homing. Bone. 2006; 38(4):497–508. [PubMed: 16337237]
37. Mun SH, Won HY, Hernandez P, Aguila HL, Lee SK. Deletion of CD74, a putative MIF receptor, in mice enhances osteoclastogenesis and decreases bone mass. Journal of bone and mineral research : the official journal of the American Society for Bone and Mineral Research. 2013; 28(4):948–59.
38. Jacquin C, Koczon-Jaremko B, Aguila HL, Leng L, Bucala R, Kuchel GA, et al. Macrophage migration inhibitory factor inhibits osteoclastogenesis. Bone. 2009; 45(4):640–9. [PubMed: 19591967]
39. Santos L, Hall P, Metz C, Bucala R, Morand EF. Role of macrophage migration inhibitory factor (MIF) in murine antigen-induced arthritis: interaction with glucocorticoids. Clinical and experimental immunology. 2001; 123(2):309–14. [PubMed: 11207663]
40. Santos LL, Dacumos A, Yamana J, Sharma L, Morand EF. Reduced arthritis in MIF deficient mice is associated with reduced T cell activation: down-regulation of ERK MAP kinase phosphorylation. Clinical and experimental immunology. 2008; 152(2):372–80. [PubMed: 18341611]
41. Leech M, Lacey D, Xue JR, Santos L, Hutchinson P, Wolvetang E, et al. Regulation of p53 by macrophage migration inhibitory factor in inflammatory arthritis. Arthritis and rheumatism. 2003; 48(7):1881–9. [PubMed: 12847682]
42. Denkinger CM, Denkinger M, Kort JJ, Metz C, Forsthuber TG. In vivo blockade of macrophage migration inhibitory factor ameliorates acute experimental autoimmune encephalomyelitis by impairing the homing of encephalitogenic T cells to the central nervous system. Journal of immunology. 2003; 170(3):1274–82.
43. Verbeke H, Geboes K, Van Damme J, Struyf S. The role of CXC chemokines in the transition of chronic inflammation to esophageal and gastric cancer. Biochimica et biophysica acta. 2012; 1825(1):117–29. [PubMed: 22079531]
44. Liao TS, Yurgelun MB, Chang SS, Zhang HZ, Murakami K, Blaine TA, et al. Recruitment of osteoclast precursors by stromal cell derived factor-1 (SDF-1) in giant cell tumor of bone. Journal of orthopaedic research : official publication of the Orthopaedic Research Society. 2005; 23(1): 203–9. [PubMed: 15607894]
45. Wright LM, Maloney W, Yu X, Kindle L, Collin-Osdoby P, Osdoby P. Stromal cell-derived factor-1 binding to its chemokine receptor CXCR4 on precursor cells promotes the chemotactic recruitment, development and survival of human osteoclasts. Bone. 2005; 36(5):840–53. [PubMed: 15794931]
46. Niwa T, Mizukoshi K, Azuma Y, Kashimata M, Shibutani T. Fundamental study of osteoclast chemotaxis toward chemoattractants expressed in periodontitis. Journal of periodontal research. 2013; 48(6):773–80. [PubMed: 23586648]
47. Im JY, Min WK, Park MH, Kim N, Lee JK, Jin HK, et al. AMD3100 improves ovariectomy-induced osteoporosis in mice by facilitating mobilization of hematopoietic stem/progenitor cells. BMB reports. 2014; 47(8):439–44. [PubMed: 24314140]
48. Suzuki K, Onodera S, Matsuno T, Kaneda K, Nishihira J. Identification of macrophage migration inhibitory factor in synovial membranes of loosened total joint replacement. Biochem Mol Biol Int. 1996; 39(3):529–37. [PubMed: 8828804]
49. Cavaillon JM. Cytokines and macrophages. Biomedicine & pharmacotherapy = Biomedecine & pharmacotherapie. 1994; 48(10):445–53. [PubMed: 7858154]
50. Calandra T, Bernhagen J, Mitchell RA, Bucala R. The macrophage is an important and previously unrecognized source of macrophage migration inhibitory factor. The Journal of experimental medicine. 1994; 179(6):1895–902. [PubMed: 8195715]
51. Zhang Q, Guo R, Schwarz EM, Boyce BF, Xing L. TNF inhibits production of stromal cell-derived factor 1 by bone stromal cells and increases osteoclast precursor mobilization from bone marrow to peripheral blood. Arthritis research & therapy. 2008; 10(2):R37. [PubMed: 18371213]

52. Wright N, de Lera TL, Garcia-Moruja C, Lillo R, Garcia-Sanchez F, Caruz A, et al. Transforming growth factor-beta1 down-regulates expression of chemokine stromal cell-derived factor-1: functional consequences in cell migration and adhesion. Blood. 2003; 102(6):1978–84. [PubMed: 12775566]

53. Chen PF, Luo YL, Wang W, Wang JX, Lai WY, Hu SM, et al. ISO-1, a macrophage migration inhibitory factor antagonist, inhibits airway remodeling in a murine model of chronic asthma. Molecular medicine. 2010; 16(9–10):400–8. [PubMed: 20485865]

54. Leung JC, Chan LY, Tsang AW, Liu EW, Lam MF, Tang SC, et al. Anti-macrophage migration inhibitory factor reduces transforming growth factor-beta 1 expression in experimental IgA nephropathy. Nephrology, dialysis, transplantation : official publication of the European Dialysis and Transplant Association - European Renal Association. 2004; 19(8):1976–85.

55. Schiraldi M, Raucci A, Munoz LM, Livoti E, Celona B, Venereau E, et al. HMGB1 promotes recruitment of inflammatory cells to damaged tissues by forming a complex with CXCL12 and signaling via CXCR4. The Journal of experimental medicine. 2012; 209(3):551–63. [PubMed: 22370717]

56. Tang D, Kang R, Zeh HJ 3rd, Lotze MT. High-mobility group box 1 and cancer. Biochimica et biophysica acta. 2010; 1799(1–2):131–40. [PubMed: 20123075]

57. Tsung A, Tohme S, Billiar TR. High-mobility group box-1 in sterile inflammation. Journal of internal medicine. 2014; 276(5):425–43. [PubMed: 24935761]

58. Zhou Z, Han JY, Xi CX, Xie JX, Feng X, Wang CY, et al. HMGB1 regulates RANKL-induced osteoclastogenesis in a manner dependent on RAGE. Journal of bone and mineral research : the official journal of the American Society for Bone and Mineral Research. 2008; 23(7):1084–96.

59. Lubetsky JB, Dios A, Han J, Aljabari B, Ruzsicska B, Mitchell R, et al. The tautomerase active site of macrophage migration inhibitory factor is a potential target for discovery of novel anti-inflammatory agents. The Journal of biological chemistry. 2002; 277(28):24976–82. [PubMed: 11997397]

60. Hussain F, Freissmuth M, Volkel D, Thiele M, Douillard P, Antoine G, et al. Human anti-macrophage migration inhibitory factor antibodies inhibit growth of human prostate cancer cells in vitro and in vivo. Molecular cancer therapeutics. 2013; 12(7):1223–34. [PubMed: 23619302]

61. Scolnik PA. mAbs: a business perspective. mAbs. 2009; 1(2):179–84. [PubMed: 20061824]

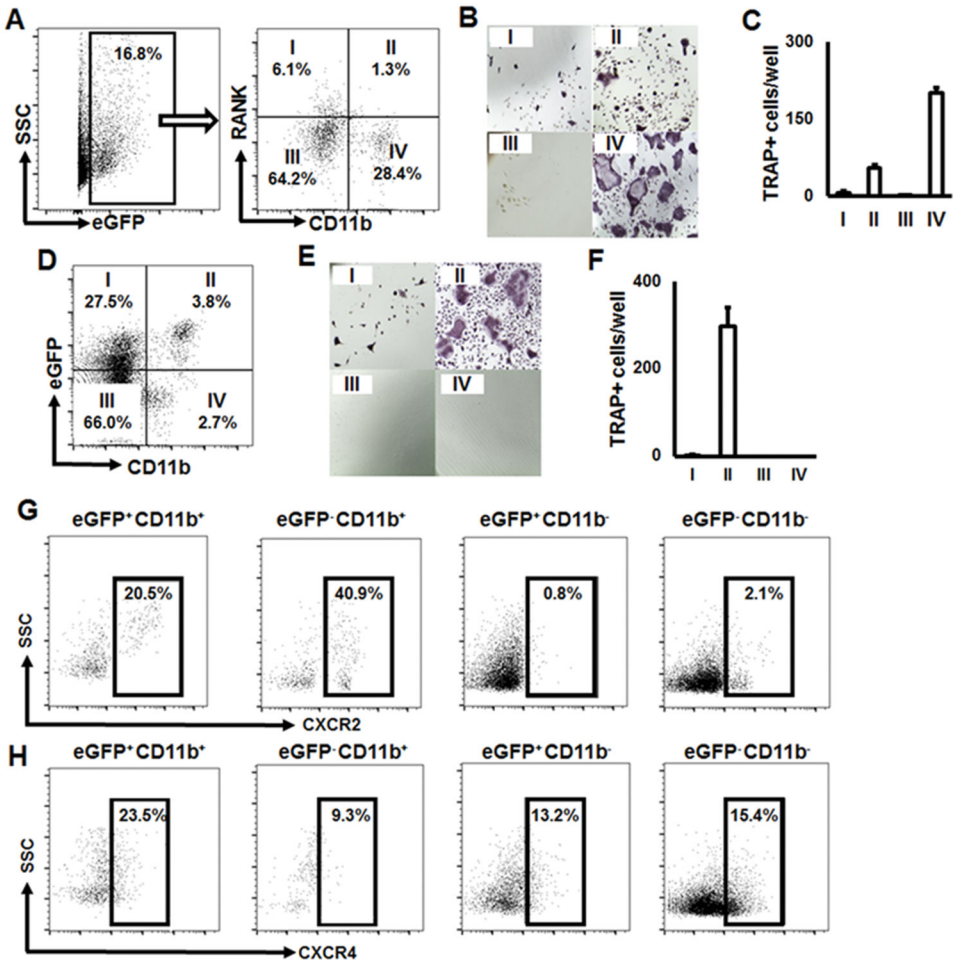

Figure 1.

OCPs have eGFP^{+}CD11b^{+} phenotype in Csf1r-eGFP-KI mice. **A)** Gated eGFP^{+}CD11b^{-}RANK^{+} (I), eGFP^{+}CD11b^{+}RANK^{+} (II), eGFP^{+}CD11b^{-}RANK^{-} (III), and eGFP^{+}CD11b^{+}RANK^{-} (IV) cell populations selected for FACS sorting. **B)** Tartrate-resistant acid phosphatase (TRAP) staining of RANKL-stimulated, FACS-sorted populations. **C)** Number of TRAP+ osteoclasts per well formed from the FACS-sorted cell populations; **D)** Gated eGFP^{+}CD11b^{-} (I), eGFP^{+}CD11b^{+} (II), eGFP^{-}CD11b^{-} (III), and eGFP^{-}CD11b^{+} (IV) selected for FACS sorting; **E)** Tartrate-resistant acid phosphatase (TRAP) staining of RANKL-stimulated, FACS-sorted populations; **F)** Number of TRAP+ osteoclasts per well formed from the FACS-sorted cell populations. **G)** and **H)** Expression of MIF congenic receptors CXCR2 and CXCR4, respectively, on the surface of FACS-sorted cell populations. Freshly isolated splenocytes were stained with anti-CD11b and anti-RANK or anti-CD11b-only Abs, FACS-sorted and then RANKL-stimulated *ex vivo*. At day 5, the cells were fixed and stained with TRAP (Sigma). TRAP+ cells with more than three nuclei were considered as osteoclasts. The number of TRAP+ osteoclasts per well are presented as mean±SD. To evaluate the expression patterns of CXCR2 and CXCR4 on the surface of eGFP^{+}CD11b^{+} OCPs, splenocytes isolated from Csf1r-eGFP-KI mice were stained with anti-CD11b, -

CXCR2, and -CXCR4 Abs. Cells were acquired on a BD FACSAria™ II Cell Sorter and analyzed by using FlowJo (ver. 10) software.

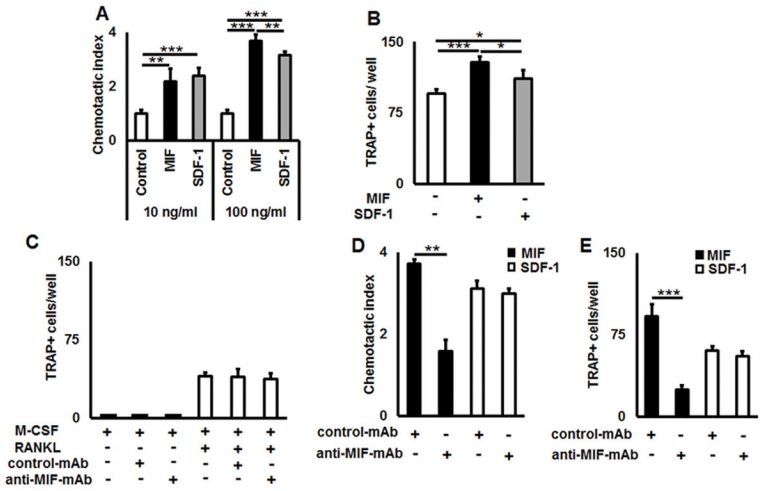

Figure 2.

MIF and SDF-1 trigger chemotactic migration of OCPs and promote osteoclastogenesis via ligation to CXCR4 receptor *in vitro*. **A)** Transmigration of FACS-sorted eGFP^{+}CD11b^{+}OCPs across the Transwell culture insert in response to various concentrations of MIF and SDF-1 chemokines. **B)** Number of differentiated TRAP+ osteoclasts differentiated from the transmigrated eGFP^{+}CD11b^{+} OCPs in response to MIF and SDF-1. **C)** Effects of anti-MIF-mAb and control-mAb on RANKL-induced osteoclastogenesis in the absence of MIF or SDF-1 chemokines. **D)** Inhibitory effects of anti-MIF-mAb, but not control-mAb, on chemotactic migration of eGFP^{+}CD11b^{+} OCPs to MIF and SDF-1. **E)** Number of TRAP+ osteoclasts per well formed from the RANKL-stimulated, transmigrated eGFP^{+}CD11b^{+} OCPs in the presence of MIF and SDF-1. Freshly FACS-sorted OCPs (5×10^{5}) were loaded in the upper chamber of a Transwell culture insert and allowed to migrate for 12 h toward the lower chamber of the transwell device that contained MIF or SDF-1 (both 100 ng/ml). The number of transmigrated cells in the lower chamber was counted microscopically. Data are expressed as chemotactic index (mean±SD) and representative of three independent experiments is shown (A). To induce osteoclastogenesis from the transmigrated OCPs in response to MIF or SDF-1, the transmigrated respective OCPs were incubated in 96 well plate (1×10^{4} cells/well) in the presence of RANKL and M-CSF (50 and 30 ng/ml, respectively) with or without MIF or SDF-1 (100 ng/ml, respectively) for 5 days. The number of TRAP+ osteoclasts per well is presented as mean±SD (B). To evaluate the possible effects of anti-MIF-mAb or control-mAb on osteoclastogenesis process, FACS-sorted eGFP^{+}CD11b^{+} OCPs were incubated with RANKL and M-CSF (50 and 30 ng/ml, respectively) in the presence or absence of anti-MIF-mAb or control-mAb (100 μg/ml, respectively) for 4 days (C). Anti-MIF-mAb or control-mAb (100 μg/ml, respectively) was also applied to the OCPs transmigration toward MIF or SDF-1 (D) and RANKL-induced osteoclastogenesis assay from the transmigrated respective OCPs in the presence or absence of MIF or SDF-1 (E) following the protocols described for (A) & (B). *p<0.05, **p<0.01, ***p<0.001.

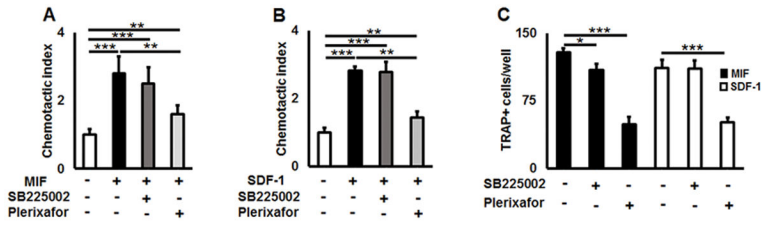

Figure 3.

MIF triggers chemotaxis of OCPs via ligation to its cognate receptor CXCR4 *in vitro*. **A)** and **B)** MIF- and SDF-1-induced chemotaxis of freshly isolated $eGFP^{+}CD11b^{+}$ OCPs, respectively, was significantly suppressed by plerixafor, a CXCR4 antagonist, but not SB225002, a CXCR2 antagonist. **C)** Number of TRAP+ cells per well induced from RANKL-stimulated, transmigrated OCPs in response to MIF or SDF-1. A chemotaxis of freshly sorted OCPs (5×10^5 cells/well) toward MIF (A: 100 ng/ml) or SDF-1 (B: 100 ng/ml) in the Transwell culture insert were incubated in the presence or absence of plerixafor or SB225002 (100 ng/ml, respectively), for 12 hours. The number of cells in the lower chamber was counted microscopically. Data are expressed as chemotactic index (mean±SD) and representative of three independent experiments is shown. To study the role of CXCR2 and CXCR4 receptors in osteoclastogenesis (D), transmigrated OCPs in response to MIF or SDF-1 were collected from the lower chamber of Transwell and subjected to osteoclastogenesis assay in 96well plate by stimulation with RANKL (50 ng/nl)/M-CSF (30 ng/ml) in the presence of respective chemoattractant, MIF or SDF-1 (100 ng/ml, respectively). To block CXCR2 and CXCR4 receptors, cells were incubated in the presence/absence of plerixafor or SB225002 (100 ng/ml, respectively) for 5 days. The number of TRAP+ osteoclasts per well are presented as mean±SD. *p<0.05, **p<0.01 ***p<0.001.

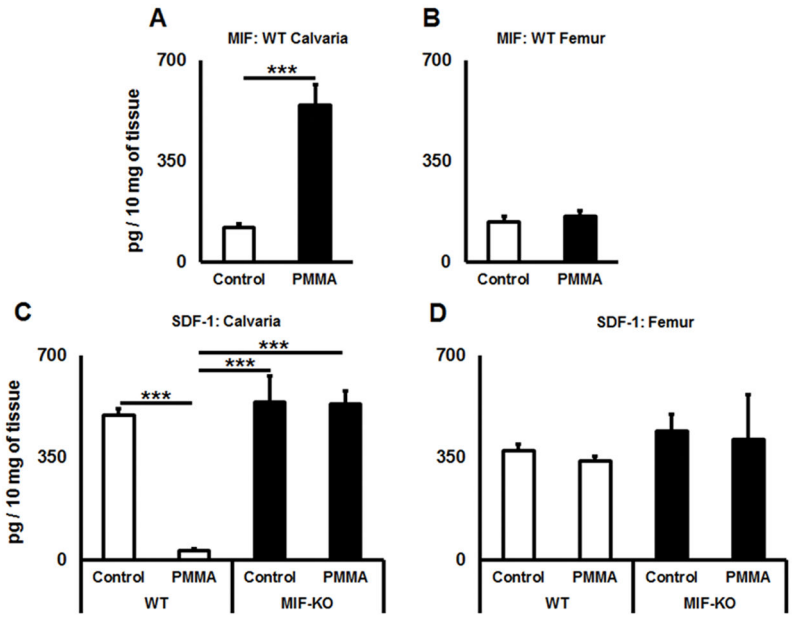

Figure 4.

A PMMA-induced osteolytic lesion has elevated level of MIF and diminished amount of SDF-1 chemokines *in vivo*. **A)** and **B)** Concentrations of MIF detected in calvaria and femur tissues of control (no particles placed) and PMMA particle-induced osteolytic calvarial lesions in WT animals; **C)** and **D)** The amounts of SDF-1 in calvaria and femur tissues of control (no particles placed) and PMMA particle-induced osteolytic calvarial lesions in WT and MIF-KO animals. PMMA particles suspended in PBS or PBS alone were placed over calvarial tissues of WT or MIF-KO animals (n=5 animals/group). At day 3, the tissues were dissected and homogenized in PBS buffer containing Tween 20. The supernatants were subjected to a sandwich ELISA. ** $p<0.01$, *** $p<0.001$.

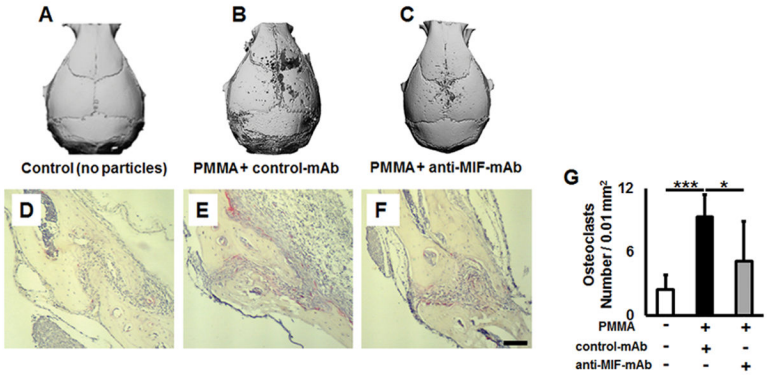

Figure 5.

Neutralizing MIF by anti-MIF-mAb reduces its negative effects in peripheral osteolytic lesions. μCT images of murine osteolytic calvarial lesions in WT animals after injection of PBS alone (**A**) and mice treated with PMMA particles in PBS over the calvarial tissue and treated i.p. with control Ab (**B**) or anti-MIF-mAb (**C**), respectively, and evaluated 7 days post-injection. **D)**, **E)**, and **F)** Histological evaluation of TRAP+ osteoclasts in calvarial sections of control (no particle placement), PMMA particle-placed and treated with control-mAb, and PMMA particle-placed and treated with anti-MIF-mAb, respectively. **G)** The number of TRAP+ osteoclasts measured in a microscopic field (0.01 mm^2) of TRAP-stained sections. A suspension of PMMA-particles (10 mg/mouse) in PBS was placed over WT murine calvariae, and immediately after particle placement, a group of animals (n=5 animals/group) were injected i.p. with anti-MIF-mAb or control-mAb diluted in PBS (1 mg/mouse, respectively). Control animals were injected with PBS alone. The tissues were dissected 7 days after particles placement and were prepared for TRAP histochemical staining. The total number of TRAP+ osteoclasts per 0.01 mm^2 was evaluated by Image J. Scale bar indicates 50 μm. *p<0.05, **p<0.01, ***p<0.001.

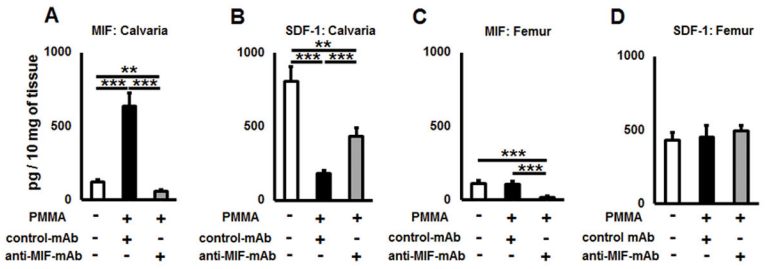

Figure 6.

Anti-MIF-mAb has a positive effect on SDF-1 levels in the PMMA-induced calvaria osteolysis lesion *in vivo*. **A)** and **B)** Concentrations of MIF and SDF-1 in dissected calvaria tissues of control (no particle placed) and PMMA particle-induced osteolytic lesions of control-mAb and anti-MIF-mAb-treated animals, respectively. **C)** and **D)** Concentrations of MIF and SDF-1 in dissected femur tissues of control (no particle placed) and PMMA particle-induced osteolytic calvarial lesions of control-mAb and anti-MIF-mAb-treated animals, respectively. A suspension of PMMA-particles (10 mg/mouse) in PBS was placed over murine calvariae, and immediately after particle placement, a group of animals (n=5 animals/group) were injected i.p. with anti-MIF-mAb or control-mAb diluted in PBS (both 1 mg/mouse). Control animals were injected with PBS alone. At day 3, the tissues were dissected and homogenized in PBS buffer containing Tween 20. The supernatants were subjected to sandwich ELISA for MIF and SDF-1. *p<0.05, **p<0.01, ***p<0.001.

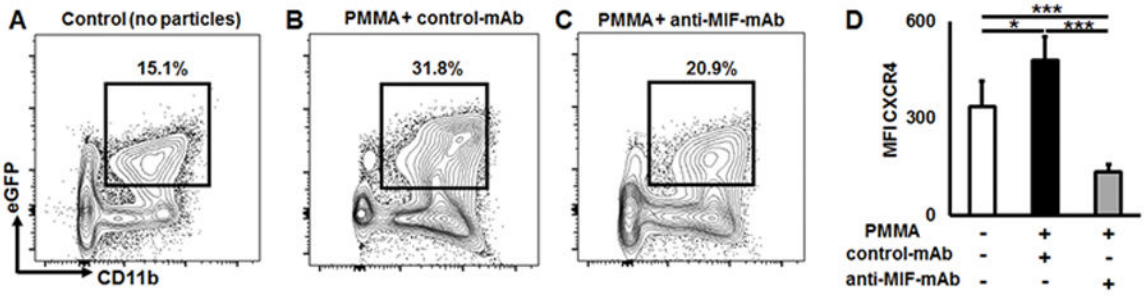

Figure 7.

Anti-MIF neutralizing mAb effectively reduces the incidence of $CXCR4^+$ OCPs in the particle-induced osteolytic lesion *in vivo*. Representative contour plots and percentage of $eGFP^+CD11b^+$ OCPs identified in peripheral osteolytic lesions induced in CSF1r-eGFP-KI mice that received **A)** control (no particles), **B)** PMMA particles + control-mAb injection, **C)** PMMA particles + anti-MIF-mAb injection; **D)** expression of $CXCR4^+$ receptor on the surface of OCPs detected in the osteolytic lesions after treatment with IgG control or anti-MIF neutralizing mAbs, respectively. PMMA particles (10 mg/mouse) suspended in PBS were placed over murine calvariae, and immediately after particle placement, the animals were injected i.p. with anti-MIF neutralizing or control mAbs diluted in PBS (both 1 mg/mouse). Control animals were injected with PBS alone. Three days after particle placement, calvarial tissues were collected and analyzed by multicolor flow cytometry. MFI: mean fluorescence intensity; $*p<0.05$, $**p<0.01$, $***p<0.001$.

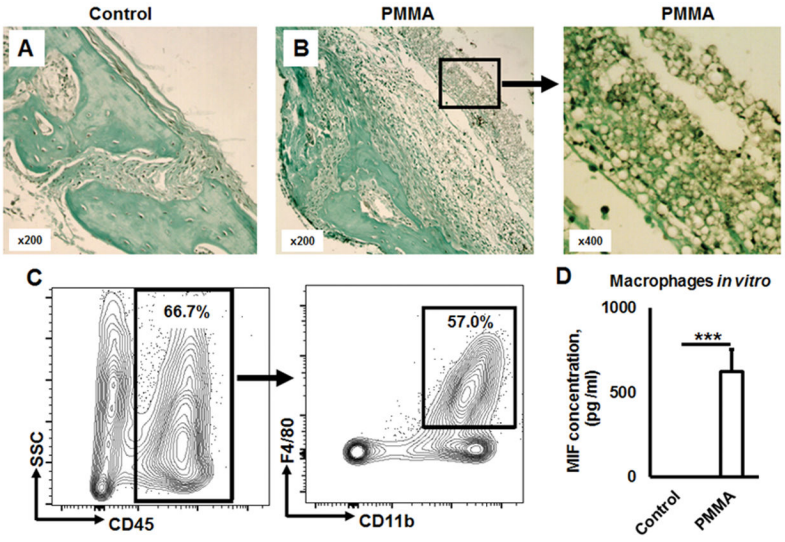

Figure 8.

Macrophages of a synovial-like periprosthetic (S-LPP) membrane are the main source of MIF in PMMA particle-induced ostelysis lesions. **A)** and **B)** Immunohistochemical detection of MIF in control (no particle placement) and PMMA-particle induced calvaria tissues, respectively. Immuno-histological evaluation of MIF-expression patterns in calvarial tissue was carried out in the WT mice that received the injection of control PBS alone or PMMA suspension in PBS for 7 days prior to the sacrifice. **C)** The percentage of macrophages gated as $CD45^{+}CD11b^{+}F4/80^{+}$ cells in dissected peri-prosthetic membranes from the PMMA-induced osteolysis lesion of WT animals (n=5/group) evaluated by multicolor flow cytometry. **D)** MIF release from bone marrow derived macrophages in response to PMMA particles stimulation *in vitro*. Bone marrow derived macrophages were stimulated *in vitro* by PMMA (2.5×10^{-3} %, w/v) in the presence of M-CSF (30 ng/ml) for 24 h. The supernatant was collected and the concentration of MIF was evaluated by ELISA. ***p<0.001.

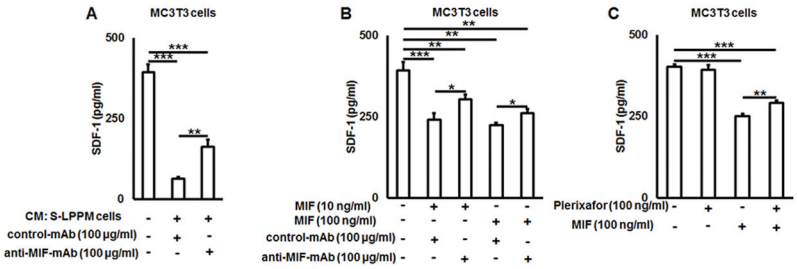

Figure 9.

MIF suppresses SDF-1 release from MC3T3 osteoblast-like cells *in vitro* in a CXCR4 dependent manner. **A)** The effects of culture medium conditioned by synovial-like peri-prosthetic membrane cells on the production of SDF-1 by MC3T3 cells in the presence or absence of anti-MIF-mAb *in vitro*. **B)** Dose response effect of mouse recombinant MIF protein in the presence or albescence of anti-MIF mAb on the production of SDF-1 by MC3T3 cells *in vitro*; C) Effects of plerixafor, a CXCR4 receptor inhibitor, on SDF-1 production from MIF-stimulated MC3T3 osteoblst-like cells. CM – conditioned media; S-LPP – synovial-like periprosthetic membrane. *p<0.05, **p<0.01, ***p<0.001.